Structures of Cytochrome *c*-549 and Cytochrome c_6 from the Cyanobacterium *Arthrospira maxima*[†,‡]

Michael R. Sawaya,[§] David W. Krogmann,[||] Ahmed Serag,[§] Kwok Ki Ho,[||] Todd O. Yeates,[§] and Cheryl A. Kerfeld*[,§]

Molecular Biology Institute, University of California, Los Angeles, Box 951570, Los Angeles, California 90095-1570, and Department of Biochemistry, Purdue University, West Lafayette, Indiana 47907

Received November 22, 2000; Revised Manuscript Received May 31, 2001

ABSTRACT: Cytochrome c_6 and cytochrome *c*-549 are small (89 and 130 amino acids, respectively) monoheme cytochromes that function in photosynthesis. They appear to have descended relatively recently from the same ancestral gene but have diverged to carry out very different functional roles, underscored by the large difference between their midpoint potentials of nearly 600 mV. We have determined the X-ray crystal structures of both proteins isolated from the cyanobacterium *Arthrospira maxima*. The two structures are remarkably similar, superimposing on backbone atoms with an rmsd of 0.7 Å. Comparison of the two structures suggests that differences in solvent exposure of the heme and the electrostatic environment of the heme propionates, as well as in heme iron ligation, are the main determinants of midpoint potential in the two proteins. In addition, the crystal packing of both *A. maxima* cytochrome *c*-549 and cytochrome c_6 suggests that the proteins oligomerize. Finally, the cytochrome *c*-549 dimer we observe can be readily fit into the recently described model of cyanobacterial photosystem II.

A *c*-type cytochrome appears to function on the donor side of all bacterial photosynthetic reaction centers. In cyanobacteria, cytochrome c_6 (also known as *c*-553) and cytochrome *c*-549 (also known as *c*-548 and *c*-550) are associated with photosystem I and photosystem II, respectively (Figure 1). The high-potential cytochrome c_6 transfers electrons from the membrane-bound cytochrome b_6f complex to photosystem I (*1*). The low-potential cytochrome *c*-549 is one of the extrinsic photosystem II subunits involved in oxygen evolution. While deletion of the gene encoding cytochrome *c*-549 results in structural instability of photosystem II, impaired growth, and diminished oxygen evolution (*2*−*5*), the role, if any, of the heme prosthetic group of cytochrome *c*-549 in oxygen evolution is unknown. Neither cytochrome *c*-549 nor cytochrome c_6 is found in higher plants. The extrinsic subunits of plant photosystem II show no homology to cytochrome *c*-549 nor do they contain heme (summarized in ref *2*). Cytochrome c_6 is replaced by plastocyanin in higher plants (*1*).

Both cytochrome c_6 and cytochrome *c*-549 appear to support multiple functions in cyanobacteria. In addition to its role in photosynthesis, cytochrome c_6 also functions in respiration, reducing cytochrome *c* oxidase (*6*, *7*). Likewise, cytochrome *c*-549 may have different functional roles depending on the physiological or environmental state of the organism. Although the gene for cytochrome *c*-549 encodes a signal sequence for targeting to the thylakoid lumen, consistent with a role as a photosystem II component, other experimental data localize cytochrome *c*-549 to the cytoplasm or to the periplasm (summarized in ref *1*). Moreover, multiple functions for the protein are consistent with observations that the abundance of cytochrome *c*-549 appears to vary with differing light conditions, the age of the culture (*8*), or the photosystem II/photosystem I ratio (*9*). For example, two populations of cytochrome *c*-549, one soluble and one membrane-bound, were detected in *Anacystis nidulans*. Both appeared to be competent in electron transfer but were distinct in their binding in ion-exchange chromatography and in EPR spectra (*10*). It has also been noted that cytochrome *c*-549 is especially abundant in dense natural blooms or commercial cultures where it is accompanied by a ferredoxin or a flavodoxin that is not found in laboratory-grown cells. This dark, anaerobic environment is similar to winter hibernation during which cyanobacteria ferment carbohydrate stores to survive. In this context, it is suggested that cytochrome *c*-549 accepts electrons from the flavodoxin/ferredoxin and reduces hydrogenase (*11*). Other proposed functions for cytochrome *c*-549 include a role similar to that of ferredoxin in cyclic photophosphorylation (*12*) or in oxidation of NADPH (*13*).

Recognition of two regions of similarity between the primary structures of cytochrome *c*-549 (∼130 amino acids) and cytochrome c_6 (∼90 amino acids) led to the suggestion that the two proteins diverged relatively recently from the same gene (*11*, *14*). A tandem arrangement of the genes for

[†] C.A.K. acknowledges the U.S. Department of Agriculture for support of this research (USDA1999-01759). M.R.S. and T.O.Y. acknowledge the support of the National Institutes of Health (Grant 31299).

[‡] Crystal structure coordinates are available from the Brookhaven Protein Data Bank (PDB): 1F1C (cytochrome *c*-549); 1F1F (cytochrome c_6); 1IGK (cytochrome *c*-549:photosystem II). The primary structure of *A. maxima* cytochrome *c*-549 has been deposited with the Protein Identification Resource (Accession Number P82603).

* To whom correspondence should be addressed. E-mail: kerfeld@mbi.ucla.edu. Phone: 310 825-7417. Fax: 310 206-3914.

[§] University of California, Los Angeles.

[||] Purdue University.

10.1021/bi002679p CCC: $20.00
Published on Web 07/10/2001

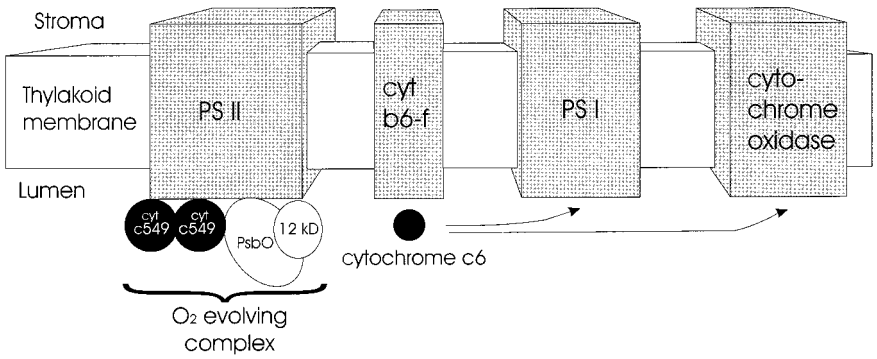

FIGURE 1: Schematic of the functions of cytochrome *c*-549 and cytochrome c_6 in cyanobacteria. In plants cytochrome *c*-549 and the 12 kDa extrinsic subunit are replaced by two nonheme proteins of 23 and 17 kDa. The electron transfer between the cytochrome b_6f complex and photosystem I is carried out by plastocyanin in plants.

cytochrome c_6 and cytochrome *c*-549 has been taken as further evidence for a gene duplication event in the evolution of these proteins (*15*). However, an ~600 mV difference between the oxidation/reduction potentials of the heme prosthetic groups of these cytochromes underscores their functional divergence. Here we report the crystal structures of both cytochrome c_6 and cytochrome *c*-549 from the same cyanobacterium, *Arthrospira* (formerly *Spirulina*) *maxima*. Cytochrome *c*-549 from *A. maxima* has a lower midpoint potential (−260 mV; *16*) than any other monoheme cytochrome of known structure. Yet we find that its structure is remarkably similar to that of *A. maxima* cytochrome c_6, whose midpoint potential is very much higher (+314 mV; *17*). Comparison of the structures of these paralogous gene products reveals several structural differences that may underlie their divergent functions and their large difference in midpoint potential. Furthermore, we find that the observed dimeric structure of cytochrome *c*-549 may relate to its function as a component of photosystem II.

MATERIALS AND METHODS

Purification and Biochemical Characterization. A. maxima cells were purchased from Earthrise Farms (Calapatria, CA). Cytochrome c_6 ("unfractionated") was purified by the method of Ho et al. (*18*). Isoforms ("monomer" and "dimer") of the protein were subsequently separated by size-exclusion chromatography on a Superose 12 and a Superose 6 column in series, equilibrated in 50 mM Tris, pH 8.0, 100 mM glycine, and 0.02% sodium azide. Elution was monitored at 280 nm. Molecular weight estimation was made by comparison to the elution behavior of a gel filtration standard mixture (Bio-Rad, Hercules, CA), to horse heart cytochrome *c* and to *Pseudomonas* cytochrome *c*-551 (Sigma, St. Louis, MO). For identification of cytochrome c_6 isoforms, samples were prepared for ion-spray mass spectroscopy by concentrating and dialyzing against 5 volumes of water in Centricon 10 concentration cells (Amicon, Beverly, MA). Mass spectrometry data were recorded at the UCLA Center for Molecular and Medical Sciences Spectroscopy.

A. maxima cytochrome *c*-549 was purified as described (*18*, *19*). The amino acid sequence was obtained by Edman degradation as described for low-potential cytochrome *c*-550 from the cyanobacterium *Microcystis aerugenosa* (*14*). Peptides were prepared by digesting the cytochrome with Endo Asp N and Endo Arg C peptidases (Boehringer, Mannheim, Germany). The resulting sequence gave a calculated mass in agreement with that determined by MALDI mass spectrometry with the correction for the mass of the heme.

Crystallization. Cytochrome *c*-549 and the fraction of cytochrome c_6 that eluted as a dimer in gel filtration were dialyzed into 5 mM Tris, pH 7.5, prior to crystallization. The final protein concentration was 10 mg/mL for cytochrome c_6 and 11.7 mg/mL for cytochrome *c*-549. Both were crystallized by vapor diffusion; the hanging drops contained a 1:1 mixture of protein and reservoir solution.

A. maxima cytochrome c_6 crystallized over a reservoir containing 0.1 M Tris, pH 7.8, 2.4 M ammonium sulfate, 0.5 M lithium sulfate, and 1% glycerol. The crystals diffracted X-rays to 2.7 Å resolution and indexed in space group $P2_12_12_1$, with unit cell dimensions of $a = 79.4$ Å, $b = 67.8$ Å, and $c = 49.7$ Å, with three molecules in the asymmetric unit.

Cytochrome *c*-549 was crystallized over a reservoir solution of 0.4 M ammonium acetate, pH 4.5, and 5% methylpentanediol (MPD).[1] The space group is $P2_1$ with unit cell dimensions of $a = 36.6$ Å, $b = 84.2$ Å, and $c = 44.2$ Å, $\beta = 95.5°$, with two molecules in the asymmetric unit.

X-ray Data Collection, Structure Determination, and Refinement. X-ray diffraction data were collected on a Rigaku RAXIS-II imaging plate equipped with an RU-200 rotating anode X-ray generator (Molecular Structure Corp., Woodlands, TX).

The structure of *A. maxima* cytochrome c_6 was solved by molecular replacement in the program AMORE (*21*) using *Chlamydomonas reinhardtii* cytochrome c_6 (*22*) as the search model. The structure of cytochrome *c*-549 was solved by molecular replacement using EPMR (*23*). Various search models based on the structure of *A. maxima* cytochrome c_6 were tested. The successful model contained 501 atoms and was based on a manual alignment of primary structures of cytochrome *c*-549 and cytochrome c_6 that assumed the *c*-549 cytochrome structure contained three helical segments common to all photosynthetic *c*-type cytochromes (*24*).

The structures of cytochrome c_6 and cytochrome *c*-549 were refined with XPLOR/CNS (*25*). The atomic models were constructed and visualized using O (*26*). Noncrystallographic symmetry (NCS) constraints were used initially in the refinement of the *c*-549 dimer, and NCS averaged difference maps were produced by RAVE (*27*). In the last

[1] Abbreviations: MPD, methylpentanediol; NCS, noncrystallographic symmetry; rmsd, root mean square deviation; PDB, Protein Data Bank.

Table 1: Data Collection and Refinement Statistics

	cytochrome c_6	cytochrome *c*-549
data collection		
resolution (Å)[a]	2.7	2.3
$\langle I/\sigma \rangle$[b]	5.0	3.3
R-merge[c] (%)	8.6	7.6
redundancy	3.2	8.4
overall completeness (%)	80.8	73.8
high res shell compl (%)	74.0	60.0
space group	$P2_12_12_1$	$P2_1$
molecules/asymmetric unit	3	2
model refinement		
R-work (%)[d]	23.2	21.7
R-free (%)[e]	25.5	26.0
weighted rmsd from ideality		
bonds (Å)	0.011	0.008
angles (deg)	1.22	1.29
average *B*-factor (Å^2)		
main chain	25.2	35.5
side chain	27.3	40.1

[a] Using all data (no $\langle I/\sigma \rangle$ cutoff). [b] $\langle I/\sigma \rangle$ is the average ratio of the observed intensity to the estimated standard deviation for the highest resolution shell. [c] *R*-merge $= 100(\sum|I_i - \langle I \rangle|/\sum_i I_i)$, where the sum is taken over the unique reflections and $\langle I \rangle$ is the mean value of the multiple measurements of the *i*th intensity. [d] *R*-work $= 100(\sum|F_o - F_c|/\sum|F_o|)$. [e] *R*-free was calculated as *R*-work using 5% of the reflections (cytochrome c_6) or 10% of the reflections (cytochrome *c*-549).

rounds of refinement, NCS constraints between the two molecules in the asymmetric unit were replaced by restraints. In the cytochrome c_6 structure, constraints between the three distinct molecules were maintained throughout refinement. Data collection and refinement statistics are given in Table 1.

RESULTS AND DISCUSSION

Quality and Completeness of the Models. All residues in the cytochrome *c*-549 and cytochrome c_6 structures fall within allowed regions of Ramachandran plots, and all residues are within the 95% confidence limit suggested by ERRAT (*28*). Due to disorder, the cytochrome *c*-549 model is missing two residues from the N-terminus and from the C-terminus, as well as side chain atoms from residues Arg105 in one molecule of the asymmetric unit and from Arg47 and Asn53 in the second molecule in the asymmetric unit. The N-terminal residue is missing from the cytochrome c_6 model. The refinement statistics are given in Table 1.

Cytochrome c_6: Overall Fold and Evidence for Oligomerization. The structure of *A. maxima* cytochrome c_6 (Figure 2a) resembles that of other algal and cyanobacterial cytochromes c_6; it is composed of four α-helices enclosing all but 6% of the surface of the heme prosthetic group (*29*). One unique feature of *A. maxima* cytochrome c_6 is an insertion of three consecutive aspartic acid residues (*44*−*46*) preceding the third α-helix (Figure 2a).

Since the crystals of *A. maxima* cytochrome c_6 were grown from a protein fraction that eluted as a dimer in gel filtration,

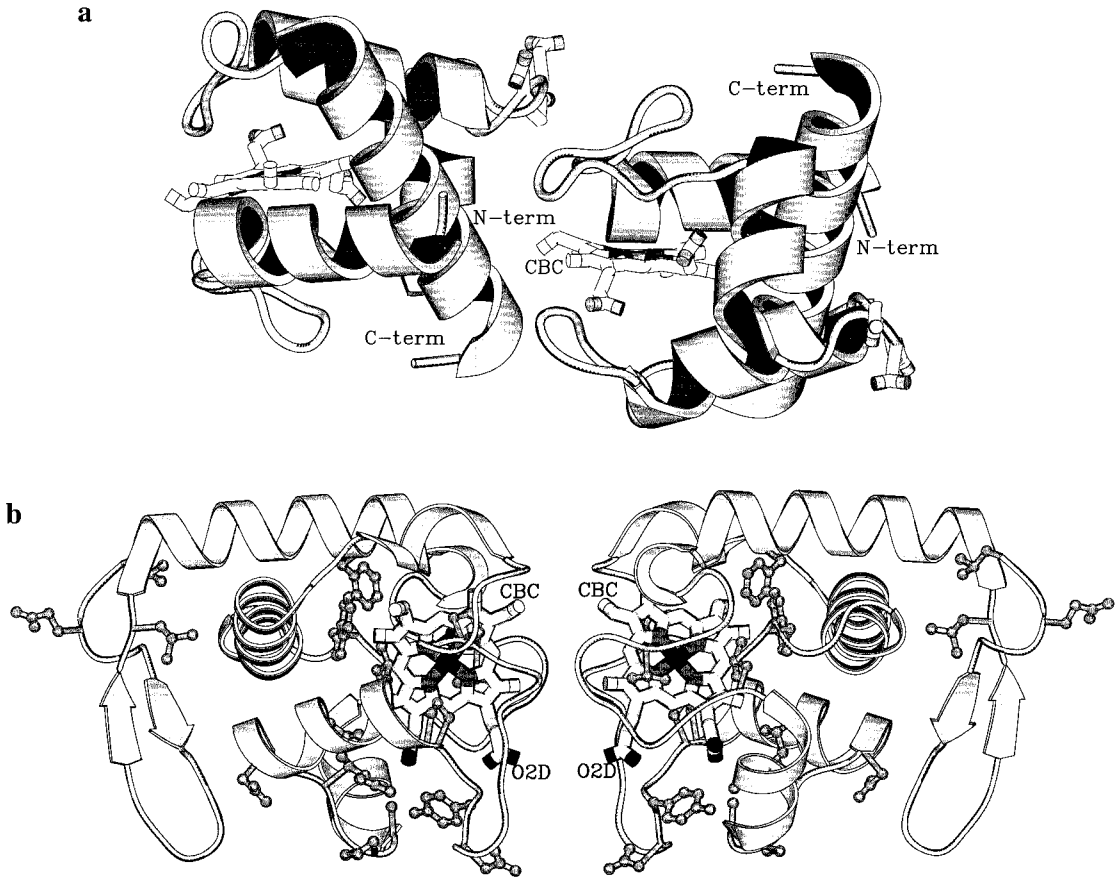

FIGURE 2: (a) Structure of *A. maxima* cytochrome c_6. Two crystallographically related molecules are shown. The side chains for residues 44−46, the insert unique to the *A. maxima* cytochrome c_6 structure, are depicted. The heme atoms with the largest surface exposure, the CBC, and propionate D oxygen atoms are labeled. The intermolecular interface involves Asp2, Val3, Ala15, Ala16, Met19, Val24, Ile25, Asp45, Asp46, Ala47, Val48, Asn60, Ala61, Lys83, and the pyrrole C edge of the heme of one of the monomers. (b) Structure of the *A. maxima* cytochrome *c*-549 dimer contained in the crystal asymmetric unit. Amino acids that are absolutely conserved in the primary structure of cytochrome *c*-549 are shown in ball-and-stick representation. This figure and Figures 3, 6, and 7 were drawn with SETOR (*53*).

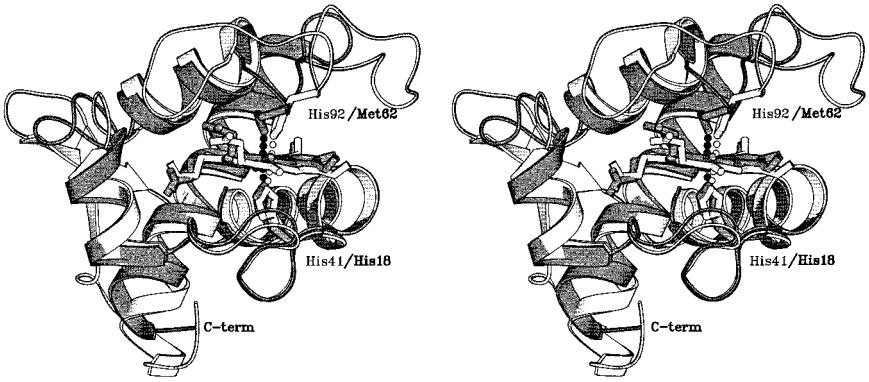

FIGURE 3: Stereo superposition of cytochrome *c*-549 and cytochrome c_6 showing axial ligands of cytochrome *c*-549 (His41 and His92) and cytochrome c_6 (His18 and Met62).

all pairwise contacts in the orthorhombic crystal were surveyed for a dimeric arrangement. In the crystal there are several distinct regions of intermolecular contact with buried surface area per monomer ranging from 188 to 481 Å^2. The largest amount of surface area buried in an intermolecular interface is between one molecule in the asymmetric unit (denoted here as molecule B) and a crystallographically related copy of molecule B (Figure 2a). This interface buries 481 Å^2/monomer or 10.1% of the surface of a cytochrome c_6 molecule. The second largest intermolecular contact within the unit cell, burying 411 Å^2 or 8.5% of the surface of cytochrome c_6, is between a distinct pair of crystallographically related molecules (A:A). The A:A interface is nearly identical to the B:B interface (all atoms of the A:A and B:B dimers superimpose with an rmsd of 0.97 Å). The amount of surface area buried in the A:A or B:B interface is comparable to that occluded in other cytochrome c_6 dimer structures: 368 Å^2/monomer in the *C. reinhardtii* "form 2" cytochrome c_6 (*22*), 386 Å^2 in the oxidized form of *Scenedesmus obliquus* cytochrome c_6 (*30*), and 334 Å^2 in *A. nidulans* cytochrome c_6 (*31*; M. Ludwig, personal communication).

In *A. maxima* cytochrome c_6 the largest interface is between molecules related by a 2-fold screw axis. The "head to tail" arrangement (Figure 2a) of a pair of cytochrome c_6 molecules results in chains of cytochrome c_6 molecules in the crystal. Ordinarily, one would discount this chaining as an effect of the 2-fold screw axis. However, since this identical type of packing occurs twice independently in the crystal (A:A and B:B), we suggest it may be a biologically relevant interaction under some conditions (e.g., high protein concentrations).

Cytochrome c-549: Overall Fold, Conserved Residues, and Comparison to Cytochrome c_6. The structure of cytochrome *c*-549 is shown in Figure 2b. Despite only 32% identity between their primary structures, the structures of cytochrome *c*-549 and cytochrome c_6 superimpose (over 263 backbone atoms) with an rmsd of only 0.7 Å (Figure 3). The structures of other class I cytochromes are far more distantly related: cytochrome *c*-549 superimposes on yeast cytochrome *c* (*32*) with an rmsd of 3.4 Å, on *Rhodobacter sphaeroides* cytochrome c_2 (*33*) with an rmsd of 4.2 Å (over 281 backbone atoms), on *Rhodopseudomonas viridis* cytochrome c_2 (*34*) with an rmsd of 3.5 Å (over 281 backbone atoms), and on *Pseudomonas* cytochrome *c*-551 (*35*) with an rmsd of 3.5 Å (over 273 backbone atoms). The structural comparison thereby reinforces the idea that these proteins with very different midpoint potentials are actually close relatives.

Table 2: Heme Atom Exposure (Å^2)

	cytochrome c_6		cytochrome *c*-549	
heme atom	monomer	B:B pair[a]	monomer	dimer[a]
CMC	16.0	3.0	0	0
CBC	28.0	0	21.0	7.0
CMD	0	0	22.0	0
CBD	0	0	3.0	0
CHD	0	0	4.0	0
O1D	4.0	4	0	0
O2D	6.0	2	21.0	8
% of surface exposed	6.3	2.0	9.7	2.7

[a] For cytochrome c_6, "pair" is defined as the A:A or B:B interface that repeats to form the cytochrome c_6 chain observed in the orthorhombic crystal forms. Only one of the two heme molecules in any pair is involved in the oligomerization interface. Calculated with areaimole (*54*) using a 1.4 Å sphere radius for solvent.

The helical core of *A. maxima* cytochrome *c*-549 is very similar to that of *A. maxima* cytochrome c_6 (Figure 2a). The longest helical segments closely superimpose on the four helices of cytochrome c_6 (Figure 3). The fold of the two proteins in the vicinity of the first axial ligand (His40 in *c*-549, His18 in cytochrome c_6) is strikingly similar (Figure 3). Cytochrome *c*-549 has an additional N-terminal 22 residues (Table 3). In part they form a short, two-stranded β-sheet that precedes the first helix and the CXXCH heme coordination sequence (residues 37−41; Table 3). A second major difference between the two structures is the insert in the primary structure of cytochrome *c*-549 that is not found in cytochrome c_6 (between residues 89 and 103; Table 3). It contains the sixth axial ligand, His92. The insert lacks secondary structure with the exception of the turn formed by residues 102−104. The protein backbone conformation in the region adjacent to the sixth axial ligand (His92 in cytochrome *c*-549, Met61 in cytochrome c_6) in the two structures is quite dissimilar (Figure 3).

Amino acids that are highly conserved in the primary structures of cytochrome *c*-549 (Table 3) cluster into three different regions of the protein. They are predominantly found in the interior of the protein, near the N-terminus, or across the bottom of the molecule in the view shown in Figure 2b. In the interior of the protein, residues Val115, Gly117, Leu120, and Lys124 appear to be important in

Table 3: *A. maxima* Cytochrome c_6 and Cytochrome *c*-549[a] Primary Structure Alignment[b]

```
A. maxima c6                                          DVAAGA SVFSANCAAC HMGGRNVIVA
                                                 20                                ^        50
A. maxima c-549 LELTEELRTF PINAQGDTAV LSLKEIKKGQ QVFNAACAQC HALGVTRTNP
A. flos. c-549  LELDETIRTV PLNDKGGTVV LSLEQVKEGK .LFNYACAQC HAGGVTKTNQ
M. aer. c-549   VELDEKTLTI TLNDAGESVT LTSEQATEGQ KLFVANCTKC HLQGKTKTNN
Syn. sp2 c-549  TALREVDRTV NLNET.ETVV LSDQQVAKGE RIFINTCSTC HNSGRTKSNP
G. theta c-549    LDENTRSV PLDDAGNTVI LTPEQVKRGK RLFNASCGQC HVGGITKTNP
P. purp. c-549    LDEATRTV PLESSGRTVV LTPEQVKRGK RLFNNSCAIC HNGGITKTNP
O. sin. c-549     LDEATRTV VADSNGNTTV LTPEQVKRGK RLFNNTCGAC HVGGVTKTNP
C. para c-549     LDEETRTV ALNST-ETVV LTPEQVKRGK RLFNSTCGIC HVGGITKTNP

A. maxima c6        NKTLSKSDLAKY LKGFDDDAVA AVAYQVTNGK NMPGFN.....
                          60                          80  ^              100
A. maxima c-549     DVNLSPEALA.. LATPPRDNIA ALVDYIKNPT TYDGFVEISE LHPSLKSSDI
A. flos. c-549      NVGLEPEALA.. GALPNR.... .....MKNPT TYDGEEEISE I.PSIKSANI
M. aer. c-549       NVSLGLGDLA.. KAEPPRDNLL ALIDYLEHPT SYDGEDDLSE LHPNVSRPDI
Syn. sp2 c-549      NVTLSLVDLE.. GAEPRRDNIL AMVDYLKNPT SYDVELDLSQ LHPNTVRADI
G. theta c-549      NLGLEPDALS.. LATPARDNIN ALVDYMKNPT SYDGLESIAE VHPSIKSADI
P. purp. c-549      NVGLDPESLG.. LATPQRDNIE ALVDYMKDPT SYDGAESIAE LHPSIKSAEI
O. sin. c-549       NVGLRPEGLS.. LATPRRDNAA ALVDYLKNPT SYDGLESIAE IHPSIKSGDI
C. para c-549       NVGLDSEALA.. LATPPRNNIE SLVDYMKNPT SYDGSEEIYD IHPSIRSADA
                                                                    ^

A. maxima c6        GR.LSPKQIE DVAAYVVDQA ..........EKGW
                                                  130
A. maxima c-549     FPKMRNISED DLYNVAGYIL LQPKVRGEQW GGGK
A. flos. c-549      F..AIAEHIL LEPLVVGTKW GGK
M. aer. c-549       YPELRNLTED DVYNVAAYML VAPRL.DERW GGTIYF
Syn. sp2 c-549      WSSMRNLNEE DLQNVSGYVL VQAQVRGVAW GGGKTVN
G. theta c-549      FPKMRSLSDE DLFAIGGHIL LQPKLSSEKW GGGKIYY
P. purp. c-549      FPKMRNLTDE DLFTIAGHIL LQPKIVSEKW GGGKIYY
O. sin. c-549       YPRMRSLTDE DLFSIAGHIL LQPKIVTEKW GGGKIYY
C. para c-549       FPKMRNLTEE DLYDIAGHIL LSPKILPSQW GGGKIYY
```

[a] The N-terminal thylakoid targeting signal has been removed. [b] Numbering is given for the *A. maxima* cytochrome *c*-549 sequence. Residues forming the three conserved α-helices in the *A. maxima* cytochrome c_6 structure are underlined. Conserved residues are in bold. A (^) is below each of the axial ligands. Organisms for which cytochrome *c*-549 sequences (Accession Numbers in parentheses) are presented are abbreviated as follows: *A. maxima, Arthrospira maxima* (P82603); *A. flos., Aphanizomenon flos-aquae* (P56151); *M. aer., Microcystis aeruginosa* (P19129); *Syn.* sp2, *Synechococcus* sp. 2 (Q55210); *G. theta, Guillardia theta* (O78454); *P. purp., Porphyra purpurea* (P51200); *O. sin., Odontella sinensis* (P49510); *C. para., Cyanophora paradox* (P48263).

stabilizing interhelical interactions. Others, Thr46, Arg47, Thr48, and Asn49, shield the pyrrole A, D, and C rings of the heme and would be surface exposed in a cytochrome *c*-549 monomer. Leu3, Glu5, Thr9, and Thr18 are surface exposed in the loop preceding the β-sheet. These and four other highly conserved hydrophobic amino acids have side chains exposed to solvent (Val73, Leu91, and Ile100). When the *A. maxima* cytochrome *c*-549 is modeled into the photosystem II structure (*38*), it appears that at least some of these residues (e.g., Thr18) appear to be important in interacting with other photosystem II subunits (Figure 4; discussed below).

The isoelectric point of cytochrome *c*-549 isolated from different cyanobacterial species is uniformly acidic (*19*). The structure of *A. maxima* cytochrome *c*-549 has an asymmetric charge distribution with pronounced positively and negatively charged surfaces (Figure 5). Conserved residues 64−68, 73−75, and 78−83 form three adjacent surface-exposed loops on the "lower" negatively charged surface of the molecule (Figures 2b and 5). In contrast, there are few (with the exception of Arg105) highly conserved residues on the "upper," positively charged surface of the dimer (Figures 2b and 5). This surface of the molecule would interact with portions of PSII protruding from the membrane surface (Figures 1 and 4). These extrinsic loops of the integral membrane subunits have not yet been modeled (*36*).

Methionine 104 is another highly conserved residue in the primary structures of cytochrome *c*-549 (Table 3). This side chain is less than 10 Å from the sixth axial ligand His92, and this may be important in the (re)folding of the protein. Non-native heme ligands are involved in horse cytochrome *c* refolding after acid denaturation (*37*, *38*). Many *c*-type cytochromes show reversible acid denaturation at low pH, and cytochrome *c*-549 is particularly labile (Krogmann, unpublished results), perhaps accounting for the difficulty in detecting and purifying it. In contrast, cytochrome c_6 is relatively stable at low pH. Since cytochrome *c*-549 and cytochrome c_6 are very similar in structure near His18 and His41 (Figure 3), the lower stability of cytochrome *c*-549 could be due to accessibility and protonation of the sixth axial ligand, His92. At pH 5.5, the low-potential cytochrome *c*-549 begins to lose its visible light absorption, and the Soret peak shifts to 392 nm. However, the protein can be refolded; addition of 100 mM Tris buffer, pH 7.8, and dithionite restores the absorption to that of the native, reduced cytochrome. Carbon monoxide has also been observed as another non-native axial ligand in cytochrome *c*-549 (*39*), suggesting that there is some flexibility in the axial ligation

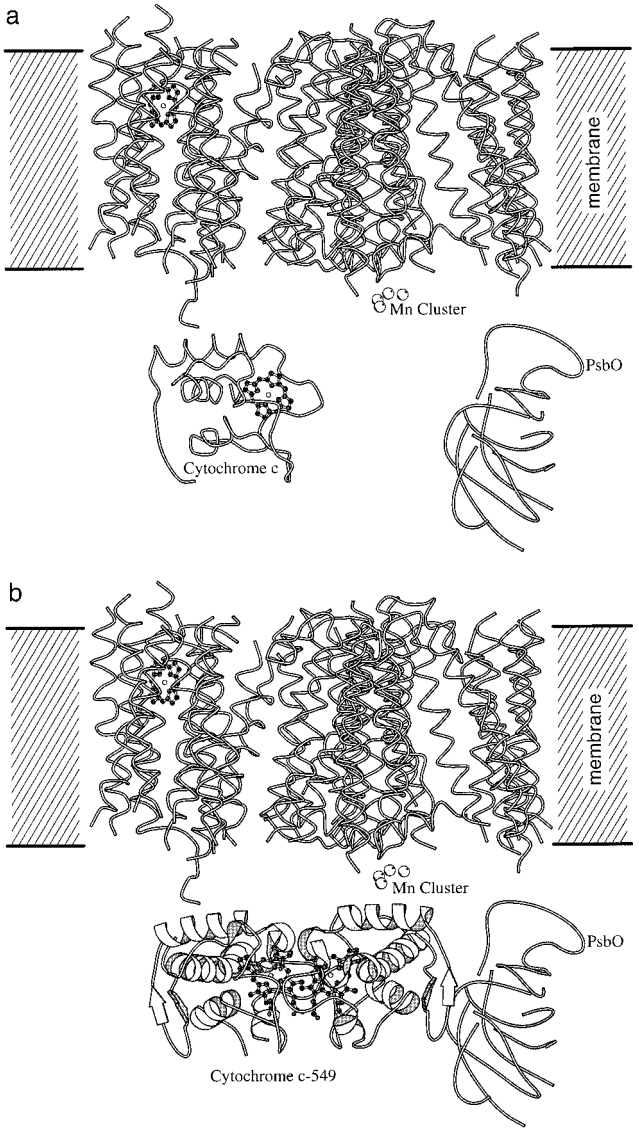

FIGURE 4: Models of the photosystem II complex. (a) The recently determined structure of PSII (*36*; PDB code 1FE1) includes one molecule of horse cytochrome *c* on the lumenal side of the complex. (b) In the model presented here, the dimer of cytochrome *c*-549 has been placed so that one protein molecule precisely overlaps the single horse cytochrome *c* molecule. This model orients the *c*-549 dimer nearly parallel to the membrane with the second molecule adjacent to the PsbO subunit. Model deposited in PDB (1IGK). Figure drawn with MOLSCRIPT (*54*).

to the heme.

Cytochrome c-549: Crystal Packing. The two molecules in the asymmetric unit of the cytochrome *c*-549 crystal are related by a 2-fold rotation axis and form a dimer across the exposed edge of the heme (Figure 2b). The dimerization buries 701 Å^2 of surface per monomer, a buried surface area comparable to that observed in known oligomer interfaces and protein−protein complexes (*40*). The distance between iron atoms in the adjacent hemes is 18.4 Å. Interprotein electron-transfer reactions typically occur across distances of 10−25 Å, suggesting that the two hemes in the dimer could interact in an electron-transfer process.

The intermolecular interface is formed by the C edge of the heme and Thr48, Asn49, Phe85, Ile88, Glu90, Leu91, and Ile100 (Figure 6); these residues are highly conserved in the primary structure of cytochrome *c*-549 (Table 3). The latter four residues are within the insert region of cytochrome *c*-549 that is not present in cytochrome c_6. The dimer interface is predominantly hydrophobic (Figure 6a), except for a hydrogen bond network formed between Thr48, Asn49, a propionate D oxygen atom, and Glu90 (Figure 6b). The side chain oxygen atoms of Glu90 are both involved in two hydrogen bonds with the adjacent molecule. A Glu/Gln or Asp residue is conserved in this position in the primary structures of low-potential cytochrome *c*-549 (Table 3), suggesting that this dimerization and this hydrogen-bonding network may be found in other cytochrome *c*-549 structures.

The cytochrome *c*-549 dimerization interface is similar in some respects to that observed in the structures of *C. reinhardtii* cytochrome c_6 (*22*), *A. nidulans* cytochrome c_6 (*31*), and *Azotobacter vinelandii* cytochrome c_5 (*41*). In each, part of the exposed edges of pyrrole ring C is buried by dimerization, with similar interatomic (CBC atom) distances (6.3 Å in cytochrome c_5, 7.9 Å in *C. reinhardtii* cytochrome c_6, 8.3 Å in cytochrome *c*-549). However, the orientation of the two molecules in the pair differs between species. For example, if a *C. reinhardtii* cytochrome c_6 monomer is superimposed on a cytochrome *c*-549 monomer, and the orientation of the second molecule in each pair is compared, a 59° rotation is required to superimpose the Cα positions of the second molecule of the two dimers. Likewise, the second molecule of the *A. nidulans* cytochrome c_6 and the *A. vinelandii* cytochrome c_5 dimer interface is rotated by 156° and 100°, respectively, relative to that of the cytochrome *c*-549 dimer.

The availability of a preliminary structure for PSII (*36*) allowed us to model the interactions of the cytochrome *c*-549 dimer with PSII. In the recently reported model, a single cytochrome molecule was placed in the complex by positioning the known structure of horse heart cytochrome *c* into the preliminary electron density map. In our model of the PSII complex, we position our cytochrome *c*-549 dimer so that one protein molecule overlaps the single horse heart cytochrome *c* molecule reported (Figure 4). This superposition was accomplished automatically using a computer program without any manual intervention or bias. Multiple lines of reasoning suggest that this resulting model of PSII with the cytochrome *c*-549 dimer may be essentially correct. Our placement of the cytochrome *c*-549 dimer puts the second protein molecule (specifically residues 15−22) adjacent to, but not overlapping, the peripheral PsbO subunit (Figure 4). The recently reported PSII model leaves a large gap between the cytochrome and PsbO, while cross-linking studies have shown that the two protein molecules are adjacent (*42*, *43*). A further circumstantial argument favors the present model. Our placement of the cytochrome *c*-549 dimer was fully dictated by the existing model and admitted no user input. Yet this placement arranges the dimer nearly flat with respect to the membrane (Figure 4). In fact, the dyad symmetry axis of the cytochrome *c*-549 dimer falls within 7° of the membrane normal (deduced from the arrangement of transmembrane helices in the PSII model). The probability of this occurring by random chance (e.g., with an incorrect or arbitrarily oriented dimer) is less than 1%. The *c*-549 dimer 2-fold is approximately parallel to the 2-fold and pseudo-2-fold axes of PSII. We must be cautious about the implications of our placement of the cytochrome *c*-549 dimer because the 12 kDa subunit has not yet been

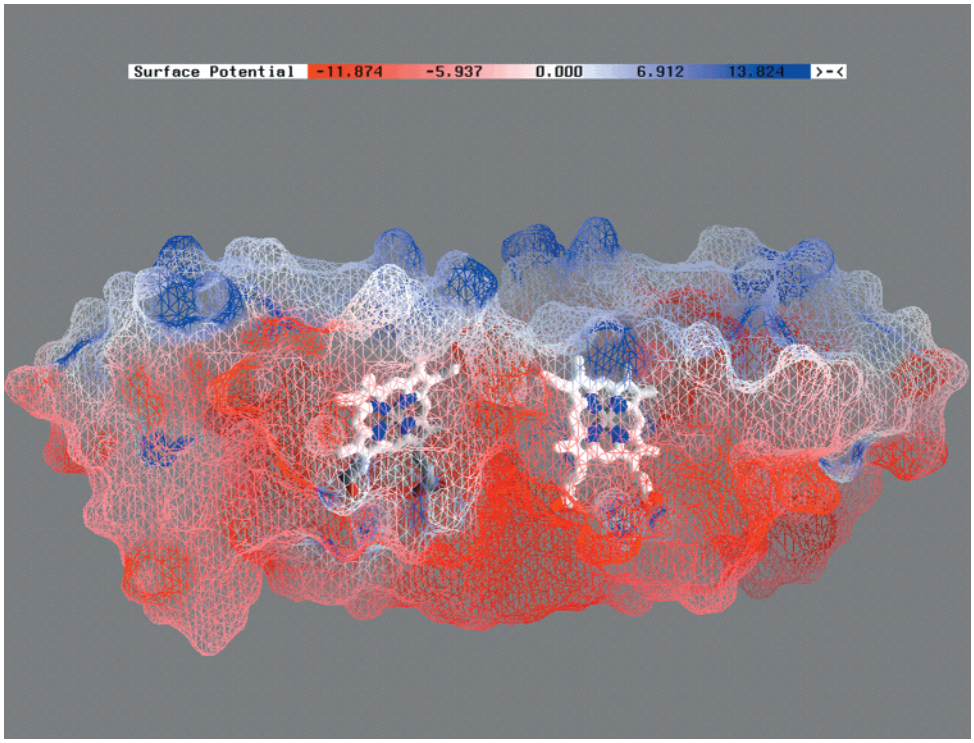

FIGURE 5: Electrostatic surface potential of the cytochrome *c*-549 dimer. The scale bar is in units of k_B, where 1 k_B = 0.6 kcal/mol. The view is approximately the same as that shown in Figure 1b. The heme prosthetic group is represented in ball-and-stick form. Electrostatic potentials were calculated using GRASP (*55*). Dielectric constants of 80 and 2 were used for the solvent and protein interior, respectively, and the ionic strength of the solvent was taken to be 0 M.

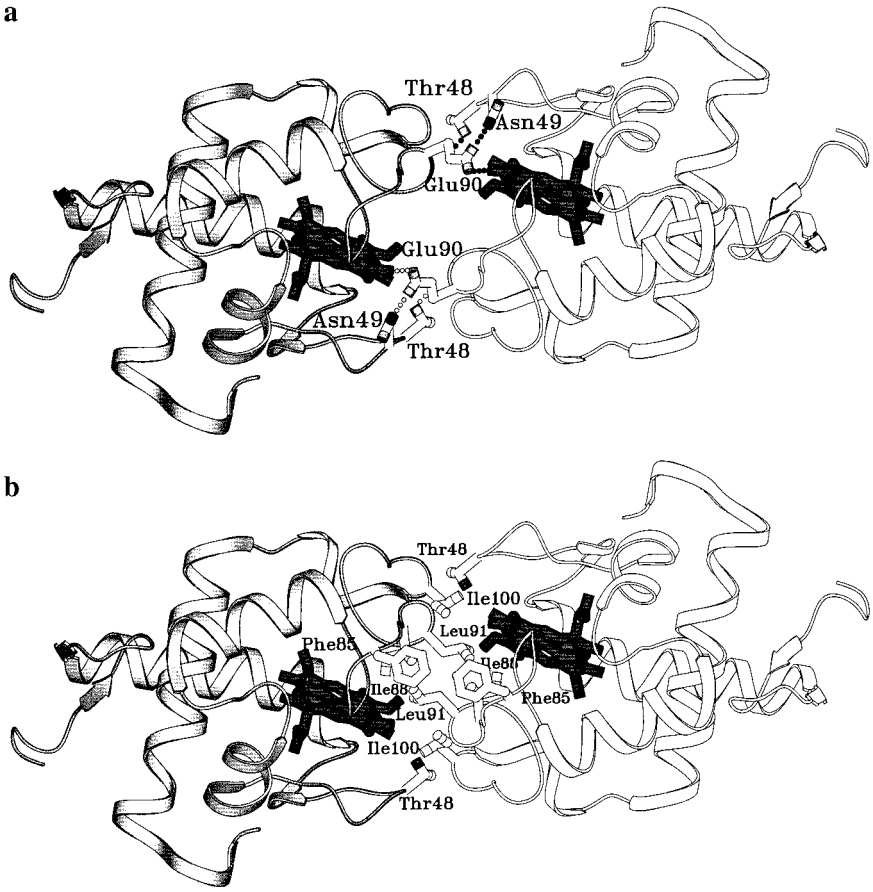

FIGURE 6: Detail of the cytochrome *c*-549 dimerization interface showing (a) the hydrogen bond network and (b) the hydrophobic core.

modeled into PSII. Nonetheless, our PSII−cytochrome *c*-549 model presents some attractive features that can now be tested experimentally.

Heme Environment and Midpoint Potential of Cytochrome c-549 and Cytochrome c_6. Despite a striking overall structural similarity, the midpoint potentials of the *A. maxima* cyto-

Table 4: Hydrogen Bonding to the Heme Propionate Oxygen Atoms and Axial Ligands

	cytochrome c_6	cytochrome *c*-549
heme atom		
O1A	none	water 614 (O) 2.8 Å
O2A	Thr30 (O) 2.5 Å	Asn53 (O) 2.5 Å
O1D	Lys59 (NZ) 2.8 Å	Tyr82 (N) 2.9 Å
		water 609 (O) 2.5 Å
O2D	Asn60 (ND2) 2.7 Å	Glu90 (OE1) 2.5 Å
	Lys59 (NZ) 3.1 Å	(in dimer only)
axial ligands		
His18/41 (NE2)	heme (Fe) 2.0 Å	heme (Fe) 2.2 Å
ND1	Arg22 (O) 2.9 Å	Val45 (O) 2.5 Å
Met62 (SD)	heme (Fe) 2.3 Å	NA
His92 (NE2)	NA	heme (Fe) 2.2 Å
His92 (ND1)	NA	Pro (O) 2.7 Å

chrome *c*-549 and cytochrome c_6 differ by nearly 600 mV. Midpoint potential is thought to be established by several factors, including the axial ligands to the heme, surface exposure of the heme, and hydrogen bonding to the propionate oxygen atoms. Comparison of the structures of cytochrome *c*-549 and cytochrome c_6 offers several structural clues to the control of midpoint potential in the two proteins. Most obviously, there is the difference in the nature of the sixth axial ligand: His92 in cytochrome *c*-549 and Met 61 in cytochrome c_6. In general, bis-histidine coordination correlates with reduced midpoint potential. Experimental substitution of methionine for histidine as the sixth axial ligand in cytochrome c_3 increases the midpoint potential by approximately 150 mV (*44*), but this accounts for only about one-fourth of the midpoint potential difference between cytochrome c_6 and cytochrome *c*-549.

The polarity of the side chains packed around the heme is also thought to be important in establishing midpoint potential (*45*). In this respect, however, the structures of cytochrome c_6 and cytochrome *c*-549 are very similar. There are several hydrophobic amino acids that are conserved structurally in the two proteins; Leu54, Leu59, and Val115 in cytochrome *c*-549 superimpose on Leu31, Leu36, Val55, and Val77 of cytochrome c_6, respectively. Buried water molecules near the heme have also been considered important with respect to electron-transfer properties (summarized in ref *46*). The buried water molecules in the cytochrome *c*-549 structure are tabulated in the Supporting Information.

Hydrogen bonding to the axial ligands is also thought to influence midpoint potential. Hydrogen-bonding interactions of the axial ligands in *A. maxima* cytochrome c_6 and cytochrome *c*-549 are summarized in Table 4. Especially interesting in the context of midpoint potential is a comparison of the hydrogen bonding to the Nδ atom of the fifth (His) axial ligand in the two structures. In cytochrome c_6 this atom forms a hydrogen bond to the carbonyl oxygen atom of Arg22; in cytochrome *c*-549 it hydrogen bonds to the same backbone atom of Val45. The backbone atoms of these two residues closely superimpose in the overlap of the structures. Electrostatic effects from the side chains of these two residues may contribute to the greater stability of cytochrome c_6 in the reduced state.

The analogous hydrogen bond to the histidine Nδ atom in cytochrome c_2 and mitochondrial cytochrome *c* is formed with the carbonyl oxygen atom of a conserved proline residue (summarized in ref *24*). It is unclear why the amino acid side chain in this position is conserved in those species. Interestingly, in cytochrome *c*-549, the carbonyl oxygen atom of conserved Pro93 (Table 3) forms a hydrogen bond with the Nδ atom of His92.

Differences in solvent exposure of the propionate D oxygen atoms might play a small role in differentiating midpoint potential. Unlike the propionate A oxygen atoms which are buried in the protein interior with similar environments (Figure 7a,b), the propionate D environment differs more substantially between the two structures (Figure 7c,d). In cytochrome *c*-549 one of the propionate D oxygen atoms is solvent exposed (Table 2). In cytochrome c_6 both of the propionate D oxygen atoms are surface exposed (Table 2) although to a lesser degree than in the algal cytochrome c_6 structures (e.g., 13.4 and 14.3 Å^2 in the *C. reinhardtii* cytochrome c_6 structures, midpoint potential = 370 mV; *22*). Thus, increased exposure of the propionate D oxygen atoms appears to correlate with increasing midpoint potential. The correlation is opposite that observed when tabulating overall heme exposure, as discussed further below.

Differences in hydrogen bonding to the propionate D oxygen atoms in the two structures may further explain differences in midpoint potential (Table 4). The cytochrome c_6 propionate D oxygen atoms are hydrogen bonded to the positively charged Lys29 and Lys59 (Figure 7c). The positive charge in the heme environment of cytochrome c_6 may help to stabilize the electron gained by reduction of the heme and so contribute to the high midpoint potential of cytochrome c_6. In contrast, the cytochrome *c*-549 propionate D oxygen atoms are hydrogen bonded to the amide backbone of Tyr82 and water (Figure 7d), affording no electrostatic balance for the reduced heme. Such trends are consistent with mutagenesis studies in which altering the electron-withdrawing character of a side chain hydrogen bonded to the propionate group can change the midpoint potential of mitochondrial cytochrome *c* by approximately 50 mV (*45*).

By the same trend, we would expect the midpoint potential to be further reduced in the cytochrome *c*-549 dimer by the introduction of an additional hydrogen bond between the propionate D oxygen atom and the side chain of Glu90 from the dimer partner (Figure 7e). This additional negative charge in the vicinity of the heme group may destabilize negative charge on the heme by further reducing the electron-withdrawing character of the immediate environment. Consistent with this trend, in *Desulfovibrio vulgaris* cytochrome *c*-553, the monoheme protein with the closest midpoint potential to cytochrome *c*-549 (+20 mV), the propionate D environment is similarly negatively charged (Figure 7f; *47*).

In general, among monoheme cytochromes, increased solvent accessibility of the heme correlates with a decrease in midpoint potential (*48*, *49*). In *A. maxima* cytochrome c_6 the surface exposure of the heme prosthetic group (6.6%) is similar to that observed in other cytochrome c_6 structures, with the edge of pyrrole ring C and the propionate D oxygen atoms the most solvent accessible (Table 2). In the cytochrome *c*-549 monomer a significantly larger portion of the heme is solvent accessible (9.7%), consistent with its lower midpoint potential. In comparison with other monoheme cytochromes, the correlation between midpoint potential and heme exposure is good. For example, *Rhodospirillum rubrum* ferricytochrome c_2 (*50*) exhibits less heme exposure (6.3%) than *A. maxima* cytochrome c_6, and predictably its midpoint

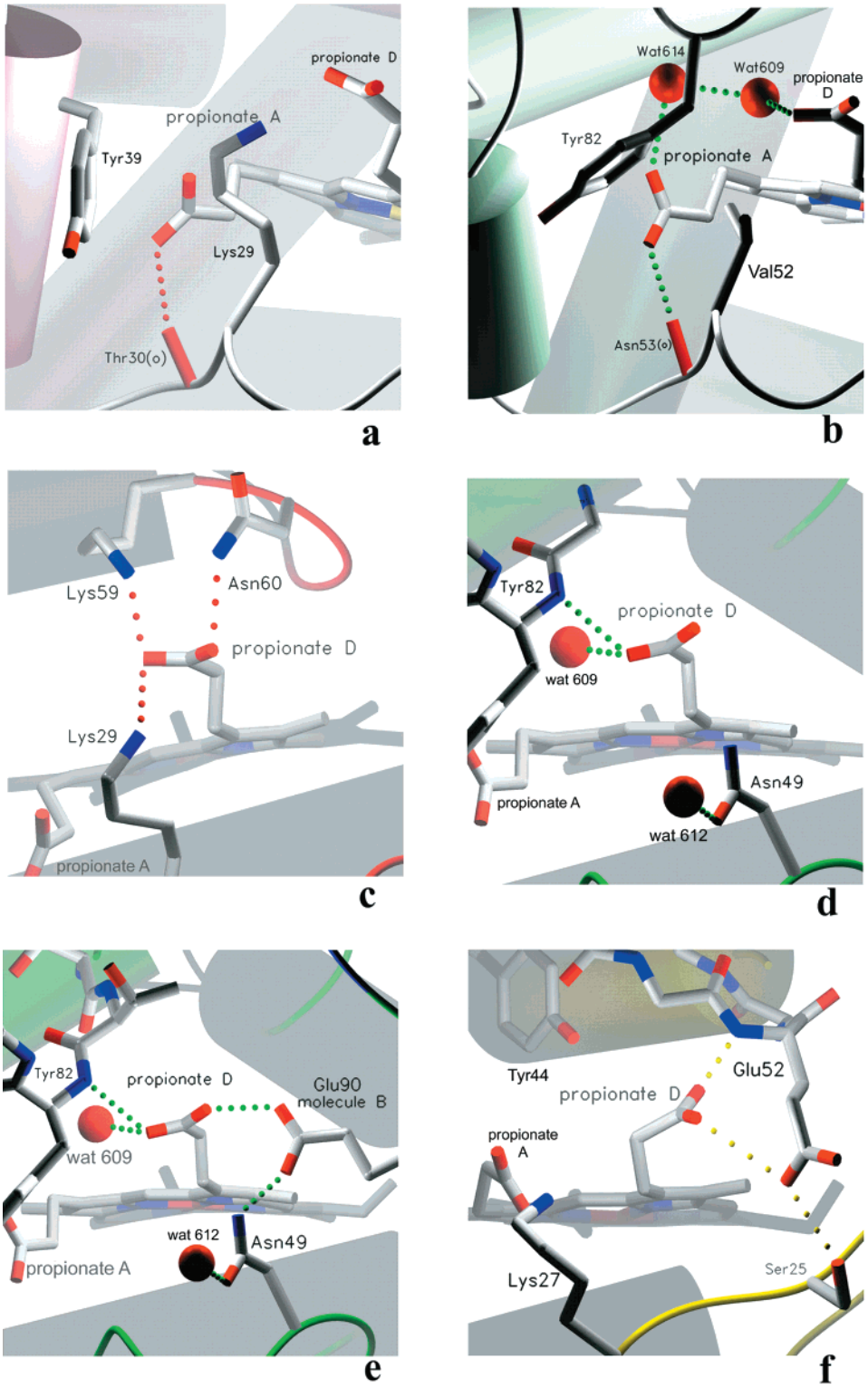

FIGURE 7: Environment of the propionate A oxygen atoms in *A. maxima* (a) cytochrome c_6 and (b) cytochrome *c*-549. (c and d) Propionate D oxygen atom environment of (c) cytochrome c_6 and (d) a monomer of cytochrome *c*-549. (e) Environment of propionate D oxygen atoms in the cytochrome *c*-549 dimer. (f) Propionate D oxygen atom environment in *Desulfovibrio vulgaris* cytochrome *c*-553 (*44*).

potential is higher (323 mV). On the other hand, correlation with multiheme cytochromes is poor; the diheme of *Desulfuromonas acetoxidans* ferricytochrome c_7 is more exposed than the heme of *A. maxima* cytochrome *c*-549, yet its midpoint potential is higher by nearly 160 mV (*51*).

If midpoint potential is critically dependent on heme exposure, we would expect the midpoint potential to increase upon dimerization of cytochrome *c*-549. Upon dimerization, exposure is substantially decreased, to 2.7% of its total surface (Table 2). The decrease in surface exposure of the heme would be expected to increase the midpoint potential of cytochrome *c*-549; however, dimerization also alters the heme environment. The aforementioned introduction of the Glu90 side chain into the heme environment as a result of dimerization (Figure 7e) may offset the effects of the loss of heme exposure upon dimerization. In addition, reduction

of one of the heme prosthetic groups in the dimer could, through electrostatic effects, depress the midpoint potential of the second heme prosthetic group. Two different midpoint potentials have been measured for cytochrome *c*-549 isolated from *A. nidulans* (*10*). The values were presumed to correspond to the membrane-bound and soluble form of the protein; the soluble protein had an oxidation−reduction potential of −260 mV whereas cytochrome *c*-549 prepared from a high-salt wash of membranes had a redox potential of ∼−300 mV. Dimerization, by affecting midpoint potential, could extend the functional range of cytochrome *c*-549 as an electron carrier.

CONCLUSIONS

It is remarkable that the cytochrome c_6 and cytochrome *c*-549 structures are so strikingly similar, given their great differences in midpoint potential. They apparently have diverged relatively recently. The oligomeric state of cytochrome *c*-549 resembles that previously observed in the structures of *A. nidulans* and *C. reinhardtii* cytochrome c_6. The dimeric structure can be placed in the context of the emerging structure of cyanobacterial photosystem II and earlier biochemical studies. The prevalence of dimers of periplasmic electron-transfer proteins and their enzymatic partners has recently been noted (*52*). A similar pattern may be emerging with respect to cytochromes involved in photosynthetic electron transport in cyanobacteria; photosystem I, photosystem II, and the cytochrome b_6f complex as well as cytochrome *c*-549 and cytochrome c_6 appear to function as oligomers.

The structure description of cytochrome *c*-549 presented here suggests a number of mutagenesis experiments to further understand its function(s) as a photosystem II component and as a redox-active protein. Furthermore, comparison of the structure to that of cytochrome c_6 reveals a number of structural differences that may underlie their very different redox properties. These observations could inform site-directed mutagenesis experiments to test hypotheses about the structural basis of midpoint potential.

SUPPORTING INFORMATION AVAILABLE

A description of the water molecules buried in the cytochrome *c*-549 structure. This material is available free of charge via the Internet at http://pubs.acs.org.

REFERENCES

1. Morand, L. Z., Cheng, R. H., and Krogmann, D. W. (1994) Soluble Electron-Transfer Catalysts of Cyanobacteria, in *The Molecular Biology of Cyanobacteria* (Bryant, D. A., Ed.) pp 243−269, Kluwer Academic, Dordrecht, The Netherlands.
2. Shen, J.-R., Ikeuchi, M., and Inoue, Y. (1992) *FEBS Lett. 301*, 145−149.
3. Shen, J.-R., and Inoue, Y. (1993) *Biochemistry 32*, 1825−1832.
4. Shen, J.-R., Vermaas, W., and Inoue, Y. (1995) *J. Biol. Chem. 270*, 6901−6907.
5. Shen, J.-R., Burnap, R. L., and Inoue, Y. (1995) *Biochemistry 34*, 12661−12668.
6. Gonzalez de la Vara, L., and Gomez-Lojero, C. (1986) *Photosynth. Res. 8*, 65−78.
7. Schmetterer, G. (1994) Cyanobacterial Respiration, in *The Molecular Biology of Cyanobacteria* (Bryant, D. A., Ed.) pp 409−435, Kluwer Academic, Dordrecht, The Netherlands.
8. Krogmann, D. W., and Smith, S. (1990) in *Current Research in Photosynthesis* (Baltscheffsky, M., Ed.) Vol. II, pp 687−690, Kluwer Academic Publishers, Boston, MA.
9. Melis, A. (1991) *Biochim. Biophys. Acta 1058*, 87−106.
10. Hogansen, C. W., Lagenfelt, G., Andreasson, L.-E., and Vanngard, T. (1990) in *Current Research in Photosynthesis* (Baltscheffsky, M., Ed.) Vol. III, pp 319−322, Kluwer Academic Publishers, Boston, MA.
11. Krogmann, D. W. (1991) *Biochim. Biophys. Acta 1058*, 35−37.
12. Kienzel, P. F., and Peschek, G. A. (1983) *FEBS Lett. 162*, 76−80.
13. Pulich, W. (1977) *J. Phycol. 13*, 40−45.
14. Cohen, C. L., Sprinkle, J. R., Alam, J., Hermodson, M. A., Meyer, T. E., and Krogmann, D. W. (1989) *Arch. Biochem. Biophys. 270*, 227−235.
15. Katoh, H., Itoh, S., Sheni, J.-R., and Ikeuchi, M. (1999) European Research Conference on the Molecular Bioenergetics of Cyanobacteria, Gmunden, Austria, June 1999, Abstract p 73.
16. Holton, R. W., and Myers, J. (1967) *Biochim. Biophys. Acta 131*, 375−381.
17. Cho, Y. S., Wang, O. J., Krogmann, D. W., and Whitmarsh, J. (1999) *Biochim. Biophys. Acta 1413*, 92−97.
18. Ho, K. K., Ulrich, E. L., Krogmann, D. W., and Gomez-Lojero, C. (1979) *Biochim. Biophys. Acta 545*, 236−248.
19. Alam, J., Sprinkle, J. R., Hermodson, M. A., and Krogmann, D. W. (1984) *Biochim. Biophys. Acta 766*, 317−321.
20. Matthews, B. W. (1968) *J. Mol. Biol. 33*, 491−497.
21. Navaza, J. (1994) *Acta Crystallogr., Sect. A 50*, 157−163.
22. Kerfeld, C. A., Anwar, H. P., Interrante, R., Merchant, S., and Yeates, T. O. (1995) *J. Mol. Biol. 250*, 627−647.
23. Kissinger, C. R., Gehlhaar, D. K., and Fogel, D. B. (1999) *Acta Crystallogr., Sect. D 55*, 484−491.
24. Kerfeld, C. (1997) *Photosynth. Res. 54*, 81−98.
25. Brunger, A. T., Adams, P. D., Clore, G. M., DeLano, W. L., Gros, P., Grosse-Kunstleve, R. W., Jiang, J. S., Kuszewski, J., Nilges, M., Pannu, N. S., Read, R. J., Rice, L. M., Simonson, T., and Warren, G. L. (1998) *Acta Crystallogr., Sect. D 54*, 905−921.
26. Jones, T. A., Zou, J. Y., Cowan, S. W., and Kjeldgaard, M. (1991) *Acta Crystallogr., Sect. A 47*, 110−119.
27. Kleywegt, G. J., and Jones, T. A. (1994) Halloween ... masks and bones, in *From First Map to Final Model* (Bailey, S., Hubbard, R., and Waller, D., Eds.) pp 59−66, SERC Daresbury Laboratory, Warrington, U.K.
28. Colovos and Yeates, T. O. (1993) *Protein Sci. 2*, 1511−1519.
29. Kerfeld, C. A., and Krogmann, D. W. (1998) *Annu. Rev. Plant Physiol. Plant Mol. Biol. 49*, 397−425.
30. Schnackenberg, J., Than, M., Mann, K., Wiegand, G., Huber, R., and Reuter, W. (1999) *J. Mol. Biol. 290*, 1019−1030.
31. Ludwig, M. L., Pattridge, K. A., Powers, T. B., Dickerson, R. E., and Takano, T. (1982) in *Electron transport and oxygen utilization* (Ho, C. H., Ed.) pp 27−32, Elsevier Science Publishers, Amsterdam.
32. Louie, G. V., and Brayer, G. D. (1990) *J. Mol. Biol. 214*, 527−555.
33. Axelrod, H. L., Feher, G., Allen, J. P., Chirino, A. J., Day, M. W., Hsu, B. T., and Rees, D. C. (1994) *Acta Crystallogr., Sect. D 50*, 596−602.
34. Sogabe, S., and Miki, K. (1995) *J. Mol. Biol. 252*, 235−247.
35. Matsuura, Y., Takano, T., and Dickerson, R. E. (1982) *J. Mol. Biol. 156*, 389−409.
36. Zouni, A., Witt, H.-T., Kern, J., Fromme, P., Krauss, N., Saenger, W., and Orth, P. (2001) *Nature 409*, 739−743.
37. Brems, D. N., and Stellwagen, E. (1983) *J. Biol. Chem. 258*, 3655−3660.
38. Sosnick, T. R., Mayne, L., Hiller, R., and Englander, S. W. (1994) *Nat. Struct. Biol. 1*, 149−156.
39. Holton, R. W., and Myers, J. (1963) *Science 142*, 234−235.
40. Jones, S., and Thornton, J. M. (1996) *Proc. Natl. Acad. Sci. U.S.A. 93*, 13−20.

41. Carter, D. C., Melis, K. A., O'Donnell, S. E., Burgess, B. K., Furey, W. F., Wang, B.-C., and Stout, C. D. (1985) *J. Mol. Biol. 184*, 279−295.
42. Han, K.-C., Shen, J.-R., Ikeuchi, M., and Inoue, Y. (1994) *FEBS Lett. 355*, 121−124.
43. Kuhl, H., Rogner, M., van Breemen, J. F. L., and Boekema, E. J. (1999) *Eur. J. Biochem. 266*, 453−459.
44. Dolla, A., Florens, L., Bianco, P., Haladjian, P., Voordouw, G., Forest, E., Guerlesquin, F., and Bruschi, M. (1994) *J. Biol. Chem. 269*, 6340−6346.
45. Cutler, R. L., Davies, A. M., Creighton, S., Warshel, A., Moore, G. R., Smith, M., and Mauk, G. (1989) *Biochemistry 28*, 3188−3197.
46. Qi, P. X., Urbauer, J. L., Fuentes, E. J., Leopold, M. F., and Wand, A. J. (1994) *Nat. Struct. Biol. 1*, 379−383.
47. Blackledge, M. J., Guerlesquin, F., and Marion, D. (1996) *Proteins: Struct., Funct., Genet. 24*, 178−194.
48. Bertrand, P., Mbarki, O., Asso, M., Blanchard, L., Guerlesquen, F., and Tegoni, M. (1995) *Biochemistry 34*, 11071−11079.
49. Tezcan, F. A., Winkler, J. R., and Gray, H. B. (1998) *J. Am. Chem. Soc. 120*, 13383−13388.
50. Salemme, F. R., Freer, S. T., Xuong, N. H., Alden, R. A., and Kraut, J. (1973) *J. Biol. Chem. 248*, 3910−3921.
51. Assfalg, M., Banci, L., Bertini, I., Bruschi, M., Giudici-Orticoni, M. T., and Turano, P. (1999) *Eur. J. Biochem. 266*, 634−643.
52. Pettigrew, G. W., Gilmour, R., Goodhew, C. F., Hunter, D. J. B., Devreese, B., Van Beeumen, J., Costa, C., Prazeres, S., Krippahl, L., Palma, P. N., Moura, I., and Moura, J. J. G. (1998) *Eur. J. Biochem. 258*, 559−566.
53. Evans, S. V. (1993) *J. Mol. Graphics 11*, 134−138, 127−128.
54. Kraulis, P. J. (1991) *J. Appl. Crystallogr. 24*, 946−950.
55. Nicholls, A., Sharp, K. A., and Honig, B. (1991) *Proteins 11*, 281−296.

BI002679P